Analysis of oscillator neural network without Lyapunov function

1999 J. Phys. A: Math. Gen. 32 4623

(http://iopscience.iop.org/0305-4470/32/25/306)

J. Phys. A: Math. Gen. **32** (1999) 4623–4640. Printed in the UK PII: S0305-4470(99)98757-7

Analysis of oscillator neural network without Lyapunov function

S Uchiyama† and H Fujisaka‡

† Department of Applied Mathematics, Hiroshima University, Higashi-Hiroshima 739-8527, Japan

‡ Department of Applied Analysis and Complex Dynamical Systems, Kyoto University, Kyoto 606-8501, Japan

E-mail: uchiyama@amath.hiroshima-u.ac.jp and fujisaka@i.kyoto-u.ac.jp

Received 27 October 1998, in final form 17 March 1999

Abstract. A new oscillator neural network is proposed on the basis of a system of coupled complex Ginzburg–Landau equations (Uchiyama S and Fujisaka H 1997 *Phys. Rev.* E **56** 99). It is shown that this network can retrieve fixed-point attractors, and has an excellent mathematical tractability (just as the Hopfield model) although the system has no Lyapunov function. We use self-consistent signal-to-noise analysis instead of the replica method to investigate the storage capacity, and demonstrate the usefulness of the present approach to the neural network exhibiting complex dynamical behaviours.

1. Introduction

Many theoretical studies have been carried out in the neural networks consisting of oscillators [1, 2], as well as in the networks of either XY spins or Heisenberg spins [3–5]. Recent neurophysiological experiments reveal the possibility that the information coded in the collective activities of neurones is described by oscillatory phenomena [6–8]. Therefore, it is quite natural to use an oscillatory element in composing a model to study such a characteristic of the neural network. Fruitful results with coupled oscillators in the last decade also encouraged research of the oscillator neural network.

Theoretical studies of the oscillator neural network commenced by using an XY spin model [9–11]. In that case, the system has a Lyapunov function. Each of the fixed-point attractors embedded in the system accurately corresponds to a minimum of the Lyapunov function, and the system evolves such that the function decreases monotonically. This property enables one to use the replica method [12], and gives the exact analytical prediction in the limit of the infinite system size, $N \to \infty$. There are variants of the above model, e.g. XY spins with native (site-dependent) frequencies, diluted couplings, slow dynamic couplings, and so on [13–16]. Moreover, there exist some theoretical models constructed with phase oscillator elements [1, 2], all of which are comprehensible by ordinary statistical-mechanical theories, assuming the existence of a Lyapunov function or something similar.

Conversely, many numerical studies have probed the complex dynamics peculiar to oscillatory systems without a Lyapunov function. Some interesting dynamical phenomena have been reported, e.g. sequential retrieval, chaotic itinerancy among patterns, and so on. We emphasize, however, the difficulty of analytically understanding such systems with the use of

0305-4470/99/254623+18$19.50

the conventional theory of statistical mechanics, because the theory requires the existence of a Lyapunov function and, moreover, these systems are generally described by quite complicated equations.

In order to conquer these difficulties we use the phase reduction method developed by eliminating the amplitude variable [17]. This is based on the approach developed in [18, 19] and gives a useful method to study the long-time dynamics of the coupled oscillator system. In the case of the global coupling term, we have numerically demonstrated the qualitative equivalence between the dynamical property of the original system [20, 21] and that of the reduced system [17]. For example, taking the complex Ginzburg–Landau (GL) equation as an element, we then construct an oscillator neural network [22] as

$$\dot{W}^{(j)} = (1 + \mathrm{i}c)W^{(j)} - (1 + \mathrm{i}c)|W^{(j)}|^2 W^{(j)} + \frac{1}{N}\sum_{k=1}^{N} D_{jk}(W^{(j)}, W^{(k)}) \qquad (j = 1, \ldots, N). \tag{1.1}$$

Here, $W^{(j)}$ is the complex physical variable at the site number j, and the parameter c is a real number. The third term in (1.1) stands for the random coupling term. If we neglect this term, each uncoupled equation has a normal form of the Hopf bifurcation. Therefore, $c \neq 0$ generates the spontaneous oscillation of elements. One may consider how to embed a number of attractors in the above system, and, if that is possible, how to predict its property analytically; however, equation (1.1) would lead to the difficulty of these problems. With the help of this phase reduction method, the system can be reduced to a quite simple one, and acquires mathematical tractability.

The goal of this paper is to analytically investigate the property of the mapping model derived from (1.1) by the reduction method. As mentioned above, there are models that are exactly solved by statistical mechanics, and those that show complex dynamics in numerical simulations. The present model has both characteristics.

This paper is organized as follows. In section 2, we propose a model, and briefly discuss its fundamental characteristics. The aim of this paper and its significance are given in section 3. In section 4, we explain self-consistent signal-to-noise analysis (SCSNA), an analytical method for the neural network that does not necessarily have a Lyapunov function. In section 5, we show the results of both numerical simulation and SCSNA. The results indicate the usefulness of SCSNA in the parameter region of small loading rate and weak nonlinearity. We summarize this paper with some remarks and conclusions in section 6.

2. Model

Let us consider a neural network system consisting of N identical oscillatory elements. We especially deal with a map element described by a phase variable θ_n ($-\pi \leqslant \theta_n < \pi$). Here the index $n = 1, 2, \ldots$ denotes a discrete time step. We suppose that, for example, the oscillator is at the firing when it passes across $\theta = 0$. Then we make the coupled map system of these oscillators, in which a variety of the firing pattern can be exhibited.

2.1. Model

In [17], we derived an oscillator neural network composed of N identical maps based on the coupled complex GL equations (1.1) by eliminating the amplitude variable. We call this model the *GL map neural network*. Each element of the system is simultaneously updated from the time step n to $n + 1$ according to

$$\mathrm{e}^{\mathrm{i}\theta_{n+1}^{(j)}} = f(h_n^{(j)}, h_n^{(j)*}) \tag{2.1a}$$

$$h_n^{(j)} = \sum_{k=1}^{N} J_{jk} \mathrm{e}^{\mathrm{i}\theta_n^{(k)}} \qquad (j = 1, \ldots, N) \tag{2.1b}$$

$$f(h, h^*) = h|h|^{-1-\mathrm{i}c}. \tag{2.1c}$$

The complex variable $h_n^{(j)}$ is the local field acting on the site j. Under its action, the phase variable $\theta_n^{(j)}$ of the jth oscillator is updated to $\theta_{n+1}^{(j)}$ by the transfer function $f(\,)$. Subsequently, $h_n^{(j)}$ is produced by summing the outputs $\mathrm{e}^{\mathrm{i}\theta_n^{(k)}}$ weighted by J_{jk}. This procedure is repeated.

Let us consider embedding $p = \alpha N$ random phase patterns, $\boldsymbol{\phi_1} \ldots, \boldsymbol{\phi_p}$, into J_{jk} such that each of them becomes an approximate fixed-point of the dynamics of $\boldsymbol{\theta_n}(=$ Col.$(\theta_n^{(1)}, \ldots, \theta_n^{(N)}))$. To this end, we can express J_{jk} with the generalized Hebb rule [9, 10] as

$$J_{jk} = \frac{1}{N} \sum_{\mu=1}^{p} \exp[\mathrm{i}(\phi_\mu^{(j)} - \phi_\mu^{(k)})] \qquad (j, k = 1, \ldots, N). \tag{2.2}$$

We choose the embedded patterns to be random and uniformly distributed in the interval $-\pi \leqslant \phi < \pi$. One readily finds that the dynamics (2.1) and the particular form of the coupling (2.2) are straightforward extensions of the Hopfield model to the oscillator network.

2.2. Characteristics of the present model

We point out how the transfer function illustrates the characteristics of the model. First, it is important to show that the transfer function has the two properties,

$$f(\mathrm{e}^{\mathrm{i}\theta} h, \mathrm{e}^{-\mathrm{i}\theta} h^*) = \mathrm{e}^{\mathrm{i}\theta} f(h, h^*) \tag{2.3}$$

$$f(\mathrm{e}^{\mathrm{i}\theta}, \text{c.c.}) = \mathrm{e}^{\mathrm{i}\theta}. \tag{2.4}$$

Equation (2.3) tells us that the system remains invariant under the rotation of its framework (*rotation symmetry*). In other words, (2.1) is never influenced by the simultaneous transformation of all phases

$$\theta_n^{(j)} \to \theta_n^{(j)} + \theta_0 \qquad (j = 1, \ldots, N).$$

Equation (2.4) indicates the set of the fixed points of the single GL map. Using this property, we can easily explain the validity of (2.2) by signal-to-noise analysis (see appendix A). Incidentally, we point out that only the difference between two phase variables is embedded in (2.2). Even if we shift each phase of the random patterns simultaneously

$$\phi_\mu^{(j)} \to \phi_\mu^{(j)} + \phi_0 \qquad (j = 1, \ldots, N, \mu = 1, \ldots, p)$$

equation (2.2) is never changed. This means that the embedded patterns ϕ arbitrarily select the origin of the framework as well as the dynamical phase variable θ.

3. Determination of retrieval region

The main aim of this paper is to investigate the dependence of the storage capacity upon the control parameter c. The loading rate α is given by $\alpha = p/N$ and the storage capacity α_c is defined as the upper limit of the loading rate. Thus, for $\alpha \leqslant \alpha_c$, the system is capable of retrieving the p $(= \alpha N)$ embedded patterns as long as the system size N is sufficiently large. For $\alpha > \alpha_c$, it is generally known that the overloading results in the collapse of all the embedded patterns.

The overlap of the system with a pattern μ

$$m_n^\mu = \frac{1}{N}\sum_{j=1}^{N} \exp[\mathrm{i}(-\phi_\mu^{(j)} + \theta_n^{(j)})] \tag{3.1}$$

is useful to characterize the state of the system. If the system stays in the state such as $|m^\mu| = \mathrm{O}(1)$ and $|m^\nu| = \mathrm{O}(N^{-1/2})$ $(\nu \neq \mu)$, the system retrieves the pattern μ, and it is said to be in a *retrieval state* (R). Alternatively, if $|m^\mu| = \mathrm{O}(N^{-1/2})$ $(\mu = 1, \ldots, p)$, the system is said to be in a *non-retrieval state* (N). Note that only the magnitude of the overlap is meaningful, since the phase of m provides no information because of the rotation symmetry of the system. Therefore, our practical goal is to determine the storage capacity $\alpha_c(c)$ at which $|m|$ is suddenly depressed. Note that we sometimes use $|m|$ to denote, if any, the largest stationary $|m^\mu|$ among $\mu = 1, \ldots, p$.

Now we briefly consider the Lyapunov function. For $c = 0$, the system reduces to the neural network that is constructed by *XY* spin elements at zero temperature. The function

$$E_n = \tfrac{1}{2}\sum_{j,k=1}^{N} J_{jk} \exp[\mathrm{i}(\theta_n^{(k)} - \theta_n^{(j)})]$$

has a lower bound, and decreases monotonically with time n. It serves as a Lyapunov function of the system, and then enables us to adopt a statistical-mechanical method, such as the replica method. It is evident from the Hermitian property of the matrix J that $E_n \in \mathbb{R}$. Taking into account the existence of this function, Cook [9] derived the storage capacity $\alpha_c(c = 0) = 0.0377$ by the replica method. On the other hand, the Lyapunov function would never exist for $c \neq 0$. Recall that the parameter c results from the nonlinear term in the complex GL equation. As is well known, there is no Lyapunov function for the complex GL equation. Therefore, it is desirable to find an analytical method for when there is no Lyapunov function.

Before starting the theoretical treatment, let us show the simulation data. Figure 1 shows some of the typical dynamics of the phase variables. We set the same p random patterns and initial phases in both figure 1(a) and figure 1(b) so as to examine the effect of c. In figure 1(a) one can recognize the rapid relaxation of the system into a phase-locked pattern, because $c = 0$ implies the existence of the Lyapunov function. On the other hand, the result in figure 1(b) looks quite different from figure 1(a). After the transient, the system oscillates temporarily around a phase-locked pattern, but this oscillation is destabilized at several sites, and that induces the attraction of the system into the other pattern at $n \simeq 350$. We confirmed numerically that the final state in figure 1(b) is sustained for a long time. This result suggests the emergence of a uniform (site-independent) frequency Ω for $c \neq 0$. The frequency will be defined later as one of the macroscopic values. In fact, its sudden change is observed at $n \simeq 350$. In figure 1(c) we present an example of non-retrieval dynamics. Because the visualization of non-retrieval state results generally in the random pattern with a high frequency, we set the special parameters at which the simulation data exhibit a small Ω (see figure 5(b)).

Now we study the dynamics of overlaps corresponding to figure 1. The results are plotted in figure 2. For $c = 0$, despite of the effect of finite size, the overlaps relax into their fixed-point values (figure 2(a)). In this case we can use the equilibrium theory. On the other hand, for $c \neq 0$, the system has no Lyapunov function, and exhibits a kind of deterministic fluctuation as observed in figure 2(b). This fluctuation plays a role of the annealing from the pseudo-attractor to the true one. In figure 2(c), all the magnitude of overlaps are $\mathrm{O}(N^{-1/2})$; however, this solution is not classified as a simple non-retrieval state because it is temporarily trapped around a pseudo fixed point approximately $310 < n < 390$. Such a state is interesting, but it is beyond the present scope of research. There may exist another non-retrieval state. Depending

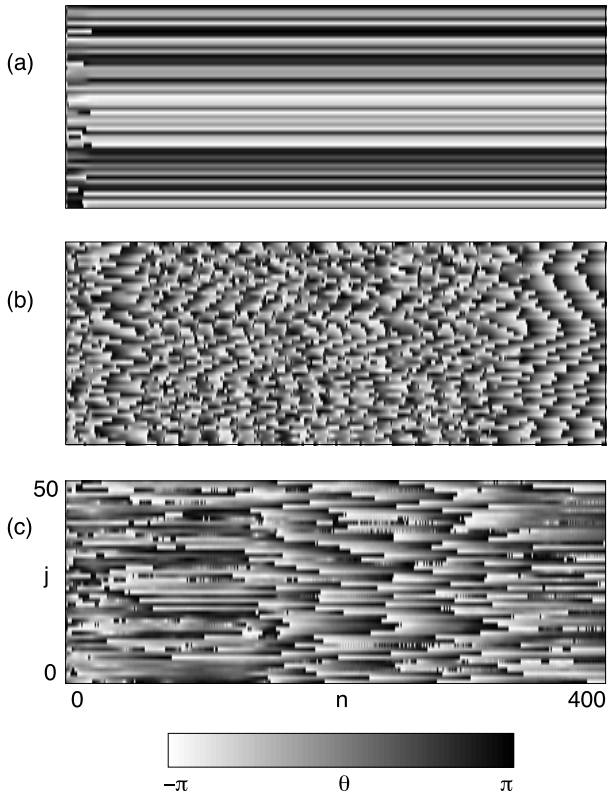

Figure 1. Dynamics of phase variables for several c and α values. Phase variables are drawn in greyscale. They are arranged into a line only for visualization. The data are produced by the simulation with $N = 1000$, the 50 sites of which are drawn. Parameter values are (*a*) $c = 0.0$, $p = 10$, (*b*) $c = 1.5$, $p = 10$ and (*c*) $c = 1.5$, $p = 40$. (*b*) Non-Lyapunov function dynamics. (*c*) An example of a non-retrieval state

on the control parameters and the initial values, the system can settle down to a 'normal' non-retrieval state like the paramagnetic one. We observe that the paramagnetic state tends to exhibit a large basin when the parameters are far from the retrieval region. Consequently, we find that the system for $c \neq 0$ can exhibit a variety of complex dynamics.

4. SCSNA

SCSNA is a statistical theory to self-consistently determine overlaps and storage capacity, developed by Shiino and Fukai. Using SCSNA, they studied the system with a non-monotonic transfer function [23]. Okuda extended their theory to the analysis of an oscillator neural network model [11], corresponding to ours with $c = 0$. He found the storage capacity $\alpha_c = 0.0377$, which is equal to that obtained by Cook using the replica method. As will be shown, SCSNA can be used even when the system under consideration has no Lyapunov function.

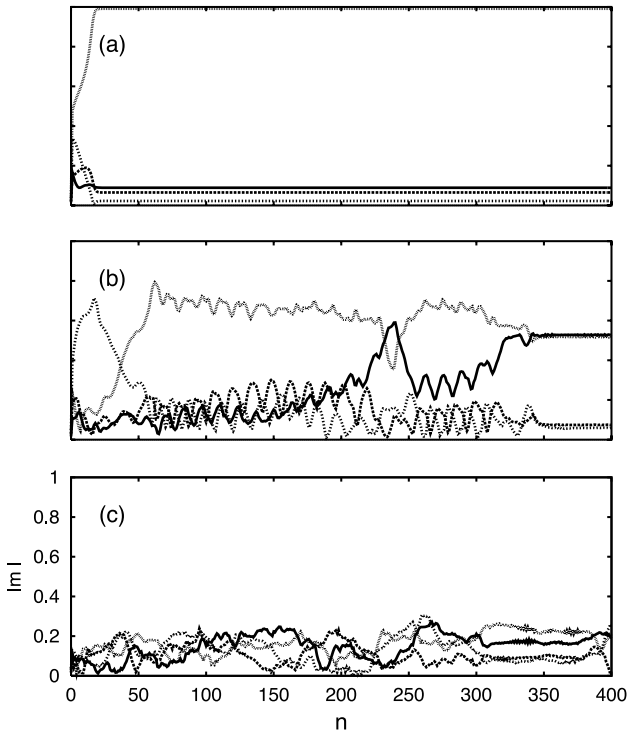

Figure 2. Dynamical behaviours of overlaps. Each overlap is calculated from the data of the corresponding part of figure 1. Only four representative overlaps are plotted. In contrast to the simple relaxation dynamics in (*a*), complicated dynamics is transiently observed in (*b*). The behaviour in (*c*) is clearly classed as non-retrieval dynamics.

4.1. General formulation

Before going into the analysis for the transfer function (2.1*c*), we first give a slightly general formulation of the complex version of SCSNA. SCSNA was originally developed as the analytic method for fixed-point attractors. We assume that the dynamics of the system settles into the embedded pattern $\mu = 1$:

$$\theta_n^{(j)} \simeq \phi_1^{(j)}. \tag{4.1}$$

The detail of the extension of SCSNA is shown in appendix B. In order to calculate the equilibrium overlap with the first pattern, we need two auxiliary macroscopic variables U and q. The macroscopic equations of SCSNA are summarized as

$$m = \langle\langle e^{-i\phi} Y(e^{i\phi}, \zeta)\rangle\rangle \tag{4.2a}$$

$$U\sqrt{\alpha r} = \langle\langle \zeta^* Y(e^{i\phi}, \zeta)\rangle\rangle \tag{4.2b}$$

$$q = \langle\langle |Y(e^{i\phi}, \zeta)|^2\rangle\rangle. \tag{4.2c}$$

Here the microscopic equation

$$Y(e^{i\phi}, \zeta) = f\left(e^{i\phi} m + \sqrt{\alpha r}\zeta + \gamma Y(e^{i\phi}, \zeta), \text{c.c.}\right) \tag{4.2d}$$

and two macroscopic relations

$$r = q|1 - U|^{-2} \tag{4.2e}$$

$$\gamma = \frac{\alpha}{1 - U} \tag{4.2f}$$

are necessary to close the above equations. The average operation is performed with respect to both the noise $\zeta = \xi + \mathrm{i}\eta$ and the random pattern ϕ:

$$\langle\langle \cdots \rangle\rangle = \frac{1}{2\pi^2} \int_0^{2\pi} \int_{-\infty}^{\infty} \int_{-\infty}^{\infty} \mathrm{e}^{-|\zeta|^2} \ldots \mathrm{d}\phi \, \mathrm{d}\xi \, \mathrm{d}\eta. \tag{4.3}$$

In terms of magnetism, m, U and q correspond to the magnetization, the susceptibility and the Edward–Anderson parameter, respectively.

4.2. Adaptation to the GL network model

Hereafter we deal with the transfer function (2.1*c*). First we point out the extension of the state for which SCSNA is useful. Instead of (4.1), we now consider the periodically oscillating pattern $\mu = 1$ with a frequency Ω,

$$\theta_n^{(j)} \simeq \phi_{\mu=1}^{(j)} + \Omega n + \theta_0 \tag{4.4}$$

since the system acquires a rotational symmetry. We put $\theta_0 = 0$ without loss of generality, and redefine the transfer function by

$$f_\Omega(\,) \equiv \mathrm{e}^{-\mathrm{i}\Omega} f(\,).$$

This makes (4.4) equal to (4.1). The property (2.3) is simply modified under this extension into

$$f_\Omega(\mathrm{e}^{\mathrm{i}\theta} h, \mathrm{e}^{-\mathrm{i}\theta} h^*) = \mathrm{e}^{\mathrm{i}\theta} f_\Omega(h, h^*). \tag{4.5}$$

Accordingly, replacing $f(\,)$ in (4.2*d*) with $f_\Omega(\,)$, we obtain a SCSNA available for the oscillating solution with a site-independent frequency Ω. Note that the identity $|f_\Omega| = |f| = 1$ yields $q = 1$. This fact decreases the number of the unknown SCSNA variables.

As is soon shown, the rotation symmetry simplifies the SCSNA equations. First, we note that (4.5) with (4.2*d*) gives

$$Y(\mathrm{e}^{\mathrm{i}\phi}, \zeta) = \mathrm{e}^{\mathrm{i}\phi} Y(1, \zeta \mathrm{e}^{-\mathrm{i}\phi}).$$

In addition, the statistics of the noise is, clearly, isotropic because of its rotational symmetry. Therefore, under the transformation $\zeta \to \zeta \mathrm{e}^{\mathrm{i}\phi}$, equations (4.2*a*) and (4.2*b*) are changed into

$$m = \langle Y(1, \zeta) \rangle \tag{4.6a}$$

$$U\sqrt{\alpha r} = \langle \zeta^* Y(1, \zeta) \rangle \tag{4.6b}$$

and when $\langle \cdots \rangle$ stands for the average over the noise $\zeta = \xi + \mathrm{i}\eta$:

$$\langle \cdots \rangle = \frac{1}{\pi} \int_{-\infty}^{\infty} \int_{-\infty}^{\infty} \mathrm{e}^{-|\zeta|^2} \ldots \mathrm{d}\xi \, \mathrm{d}\eta.$$

It is worth stressing that (4.6*a*) and (4.6*b*) ensure the non-vanishing of these macroscopic variables when averaging over ϕ.

Secondly, we mention that the argument of the overlap is arbitrarily chosen. From the definition of m, $\arg m$ is not invariant under the rotation of the framework. In fact, when a simultaneous transformation is applied

$$Y \longrightarrow Y \mathrm{e}^{\mathrm{i} \arg m} \qquad \zeta \longrightarrow \zeta \mathrm{e}^{-\mathrm{i} \arg m}$$

(4.6*a*) is changed into

$$|m| = \langle Y(1, \zeta) \rangle \tag{4.7}$$

(4.6*b*) being unchanged. This implies the complete elimination of $\arg m$ from SCSNA. Under the above transformations, (4.2*d*) is rewritten as

$$Y(1, \zeta) = f_\Omega \left(|m| + \sqrt{\alpha r}\zeta + \gamma Y(1, \zeta), \text{c.c.} \right) \tag{4.8}$$

with the help of (4.5). Here it is significant to note that the right-hand side of (4.7) must be a positive real number. This gives a condition to determine Ω.

Finally, recall the restriction of the output Y, $|Y| = 1$. Although (4.8) is a complex equation, this can be replaced by a real equation by introducing a new variable $\psi(\zeta) \equiv \arg Y(1, \zeta)$. Consequently, the present SCSNA equations are summarized as

$$|m| = \frac{1}{\pi} \int \mathrm{e}^{-|\zeta|^2} \mathrm{e}^{\mathrm{i}\psi(\zeta)} \mathrm{d}\zeta \tag{4.9a}$$

$$U\sqrt{\alpha r} = \frac{1}{\pi} \int \mathrm{e}^{-|\zeta|^2} \zeta^* \mathrm{e}^{\mathrm{i}\psi(\zeta)} \mathrm{d}\zeta \tag{4.9b}$$

$$\psi(\zeta) = g\left(|m| + \sqrt{\alpha r}\zeta + \gamma \exp[\mathrm{i}\psi(\zeta)]\right) - \Omega \tag{4.9c}$$

$$\gamma = \frac{\alpha}{1 - U} \tag{4.9d}$$

$$r = |1 - U|^{-2}. \tag{4.9e}$$

Here the transfer function $g(\,)$

$$g(h) = \arg h - c \ln |h| \tag{4.10}$$

has been defined. The above equations contain four unknown variables, $|m|$, Ω and the real and imaginary parts of U for a set of given control parameters (c, α).

4.3. Mapping criterion

Equation (4.9*c*) may, generally, have several solutions of $\psi(\zeta)$. In this situation, it is indispensable to determine which solution is realized in SCSNA. Shiino and Fukai determined the solution by using the so-called Maxwell rule in their original SCSNA. This is an inference from the minimization of the free energy. However, the Lyapunov function (the free energy in a non-stochastic system) does not exist in our model. Hence we need to develop another criterion to single out the relevant solution in (4.9*c*).

We propose the criterion as follows. We assume that if the system is on a fixed-point attractor, all the variables in SCSNA except a microscopic variable $\psi(\zeta)$ are constant. For example, in (4.9*c*), the constant variables are m, r, γ, Ω and another microscopic variable ζ. Our idea is to focus on the dynamical stability of the fixed point of $\psi(\zeta)$. Under this assumption, a specified ζ in the SCSNA representation corresponds with a specified oscillator in the simulation representation. Consequently, we can regard equation (4.9*c*) at a specified ζ as that governing the dynamics of a corresponding oscillator:

$$\psi_{n+1}(\zeta) = g\left(|m| + \sqrt{\alpha r}\zeta + \gamma \exp[\mathrm{i}\psi_n(\zeta)]\right) - \Omega. \tag{4.11}$$

According to the one-dimensional map theory, we impose the following criterion upon SCSNA (the *mapping criterion*):

- Stability of an oscillator: for a fixed ζ, $\psi(\zeta)$ is the stable solution of (4.11) if $|\frac{\mathrm{d}g(h)}{\mathrm{d}h}| < 1$ is satisfied at $\psi(\zeta)$. If there are several stable solutions, the $\psi(\zeta)$ is realized at which $|\frac{\mathrm{d}g(h)}{\mathrm{d}h}|$ is smallest.
- Stability of the system: the overall measure with no stable solution should satisfy the condition

$$\frac{1}{\pi} \int_{\text{no stable solution}} \mathrm{e}^{-|\zeta|^2} \mathrm{d}\zeta \ll 1. \tag{4.12}$$

The left-hand side of (4.12) is interpreted as the magnitude of the (deterministic) noise added to the fixed-point solution of SCSNA. It is beyond SCSNA to estimate the magnitude in which the system remains stable. This criterion is a necessary condition for a system with a large degree of the freedom to remain stable.

5. Results

5.1. Solution of the SCSNA equations

First, we briefly explain the numerical algorithm used to solve the SCSNA equations. It consists of three nested loops. The outermost loop is for the convergence of the root of the coupled equations of the SCSNA. To find the root, we used the multiple Newton method. The next loop is for the convergence of the numerical integration. It is necessary to know the integrated values at every iteration step of the multiple Newton method. There are twenty integrations in all, namely the real and imaginary parts of the right-hand sides of both (4.9*a*) and (4.9*b*) and their derivatives by the four macroscopic variables ($4 + 4^2 = 20$). We used the trapezoidal integration rule without any integral transformation. The total number of reference points for the numerical integration is typically $O(10^6)$. The innermost loop is for the convergence of the solution of (4.9*c*). For this, we used the Newton method for a single variable. After the third convergence, the mapping criterion is applied at each reference point ζ.

Now we report the result of the SCSNA calculation. Without loss of generality, c is chosen to be positive. In figure 3, we depict the $m - \alpha$ curves of the SCSNA solution for three values of c. Note that only the curve for $c = 0$ is predictable from the replica theory. This result reveals that, even for $c \neq 0$, the transition behaviours are the same as for $c = 0$. The storage capacity α_c is given by the α value where $\mathrm{d}|m|/\mathrm{d}\alpha$ diverges. For different c values, one obtains α_c–c curves. The phase diagram of the system showing the retrieval and non-retrieval regions is shown in figure 4. One observes that, near $c = 0$, the storage capacity is more enhanced when there exists no Lyapunov function ($c \neq 0$) than when the function does exist ($c = 0$). Further increase of c results in the vanishing of α_c. The increase of α_c near $c = 0$ seems to be a paradoxical result.

This paradoxical result can be interpreted as follows. As one can see in (4.10), the argument of h can be neglected for large $|c|$. In view of the local field h, large $|c|$ deforms our oscillator neural network into a kind of analogue neural network. Thus the deviation of c from zero changes the storage capacity of this model from 0.037 7 (Noest model) to

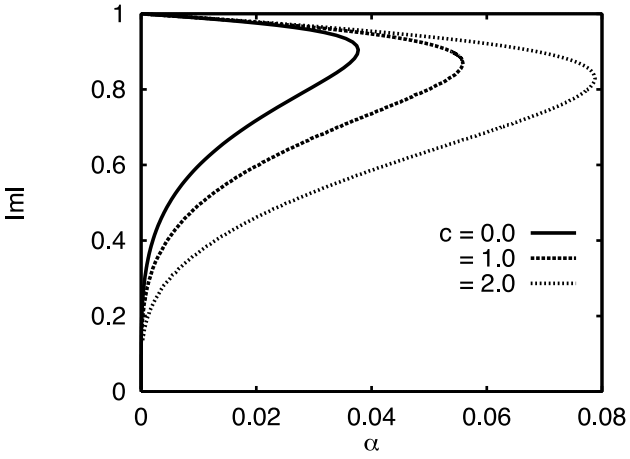

Figure 3. Dependences of the overlap m on the loading rate α for some fixed c. These are solutions of a set of SCSNA equations. Each curve has two branches, which vanish simultaneously at α_c. In the case of $c = 0$ where the system has a Lyapunov function, the branch with larger $|m|$ corresponds to its minimum and the other, to the maximum.

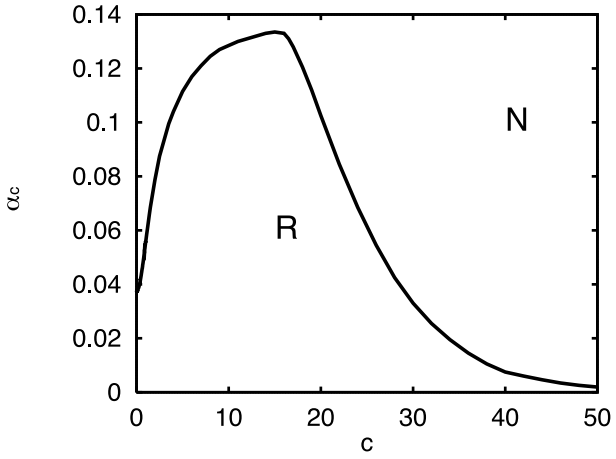

Figure 4. Analytically predicted phase diagram. The storage capacity $\alpha_c(c)$ is determined as in figure 3. The letters R and N denote retrieval and non-retrieval regions, respectively. Particularly in the vicinity of $c = 0$, it is clear that $\alpha_c(c)$ increases with c.

possibly 0.138 (Hopfield model at zero temperature). On the other hand, it is expected that α_c decreases asymptotically to zero in the limit $c \to \infty$, because the extremely large c enhances the dynamical instability of the retrieval solution. Although these two tendencies competitively contribute, the SCSNA result illustrates that the former overcomes the latter in the neighbourhood of $c = 0$.

5.2. Numerical simulations

5.2.1. Macroscopic variables. Numerical simulation is carried out for $N = 500$, and how the four macroscopic variables depend upon (c, α) is examined. The overlap m_n at time n is governed by (3.1) with the help of $\theta_n^{(j)} (j = 1, \ldots, N)$. In the same way, the susceptibility U_n is calculated from (B.7) and (B.15). Taking into account (3.1) and (4.4), we define the frequency Ω_n by

$$\Omega_n = \arg(m_n / m_{n-1}).$$

In general, these variables do not necessarily converge to finite values in the course of time. Furthermore, the attractor depends on the initial phases besides the parameters c and α. Therefore, for fixed parameters, we took the time average of the variables for the different 100 initial conditions after the transients have decayed. We then derived the ensemble average from these time averages. The initial value of $\boldsymbol{\theta_0}$ is set to be one of the embedded patterns, namely, $|m_0|$ to be exactly equal to unity. If the overlap decays ($|m| \sim 0$), the trial fails to a non-retrieval solution; otherwise the state corresponds to the retrieval of a periodic solution, following (4.4).

The results are shown in figure 5. In figure 5(*a*), the dark area shows the numerically obtained retrieval region and the light area, the non-retrieval one. The dashed curve in figure 5(*a*) is a part of the curve in figure 4. It lies precisely on the boundary of the two regions, near $c = 0$. This proves that SCSNA gives quantitatively good prediction of the simulation data for small c. On the other hand, the simulation data show the peak of α_c at $c \simeq 1$ and the rapid contraction of the retrieval region for $c \gtrsim 1$. The numerically obtained retrieval region is within that derived by SCSNA. In order to clarify to what extent SCSNA is

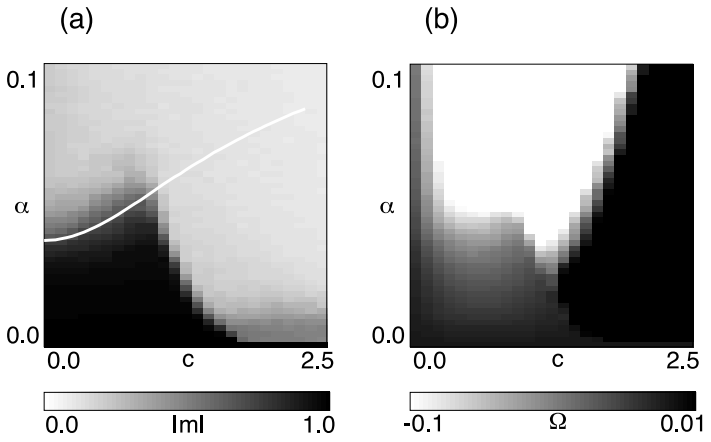

Figure 5. Numerically obtained macroscopic variables. Simulation was carried out for $N = 500$, and the average over different 100 runs is shown for (*a*) $|m|$ and (*b*) Ω. (*a*) The numerically obtained phase diagram. For comparison, the result in figure 4 is superimposed on (*a*) by the dashed curve. The greyscale range in (*b*) is adjusted so as to emphasize the dependence within the retrieval region.

successful, we plot m–α curves with simulation data in figure 6. One can see the coincidence between theory and simulation for $c = 0$. This figure makes it clear that the coincidence near α_c declines with the increase of c. The finite value of c induces the complex dynamics of the system. Since SCSNA does not include the effect of the dynamical correlations, the discrepancy between the SCSNA result and the numerical simulation becomes remarkable for large c.

5.2.2. Mapping criterion. Now let us verify the validity of the mapping criterion for the simulation with $N = 1000$. At first, we numerically sought a fixed-point solution. We calculated the stationary values of macroscopic variables from such a solution. With the help of these values, we translate the simulation data into a form suitable for SCSNA representation, and obtain the set of $\psi^{(j)}$ and $\zeta^{(j)}$ ($j = 1, \ldots, N$). A realization for $c = 1.0$ and $\alpha = 0.04$ yields figure 7(*a*), in which $\psi^{(j)}$ are plotted on the ζ plane.

The distribution of the noise has been normalized through (4.9*e*). Thus, it is certainly expected that most of the points are inside $|\zeta^{(j)}| = 1$ for $N = 1000$. For $N \to \infty$, the blank area in figure 7(*a*) vanishes. On the other hand, with the help of the same macroscopic variables, the mapping criterion makes (4.9*c*) a function of ζ, and produces figure 7(*b*), which should be compared with figure 7(*a*). If $c = 0$, $\psi(\zeta)$ is merely along the direction of the local field, namely, the curves $\psi(\zeta) = \text{const.}$ are aligned radially with the centre $\zeta = -|m|/\sqrt{\alpha r}$. Thus, if $c \neq 0$, the above radial arrangement is distorted and forms a spiral as in figure 7(*b*); the small blank region corresponds to the singular region in which the mapping criterion predicts no stable $\psi(\zeta)$. We point out that this region is far from $\zeta = 0$ and that condition (4.12) is satisfied. However, a comparison of figures 7 (*a*) and (*b*) shows that this region is not covered by the simulation with $N = 1000$. It is difficult to actually observe a phenomenon related to the singularity.

Another realization for $c = 1.5$ and $\alpha = 0.01$ is plotted in figure 8. In this example, the equilibrium state is unfortunately, classified, to the so-called spurious state. This is beyond the present SCSNA; hence the distribution of the noise is not well normalized. Nevertheless the mapping criterion works successfully. Consequently, because figure 8(*a*) qualitatively

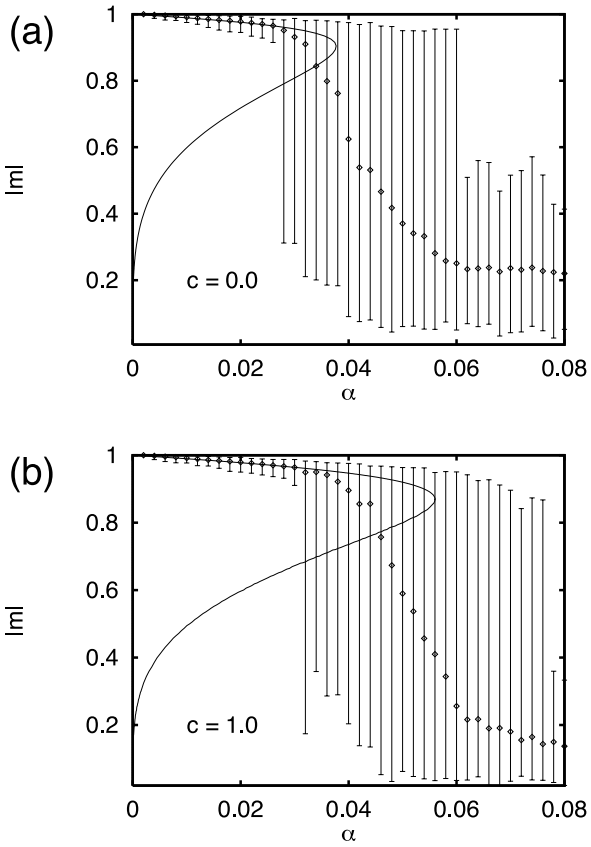

Figure 6. Comparison of m–α curves by SCSNA approximation with numerical simulations for (*a*) $c = 0.0$ and (*b*) $c = 1.0$. The symbol ($\diamondsuit$) stands for the mean value of $|m|$, and the error bar indicates the range numerically obtained. It is inevitable, due to the finite-size effect of the system, that the drastic transition around α_c does not appear in simulation data.

coincides with the centre parts of both figures 7(*b*) and 8(*b*), $\psi(\zeta)$ determined by the mapping criterion seems to be consistent with that obtained by simulation.

6. Concluding remarks

We extended SCSNA to the analysis of the oscillator neural network without Lyapunov function, and developed a mapping criterion that is an intrinsic rule to determine a fixed-point solution of the system concerned. In our formulation, it is a remarkable finding that the spontaneous frequency Ω is involved in SCSNA as one of the macroscopic variables. If we select a transfer function different from (2.1*c*), we can analyse the model by almost the same approach as long as the function has rotation symmetry.

We make some remarks about the mapping criterion. This criterion becomes plausible under the condition that the system is described not by differential equations, but by coupled maps, and moreover that the transfer function is not a linear combination of step-functions. Accordingly, in the case of the analogue neural network model with $f(h) = \tanh(\beta h) h \epsilon \mathbb{R}$), SCSNA with our mapping criterion yields the same result known so far.

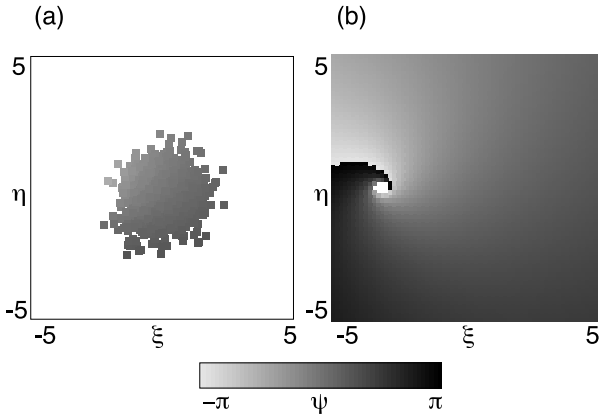

Figure 7. Validity of mapping criterion for $c = 1.0$ and $\alpha = 0.04$. (*a*) Result of the simulation for $N = 1000$. Output $\psi(\zeta)$ is drawn by greyscale as a function of noise $\zeta = \xi + i\eta$. All the variables were obtained by a numerical simulation, and translated into a form suitable for SCSNA. Note that the finite size simulation allows for blank regions that have no data. (*b*) Result of mapping criterion. Output $\psi(\zeta)$ is determined by the mapping criterion with the help of the macroscopic variables that were numerically obtained in (*a*).

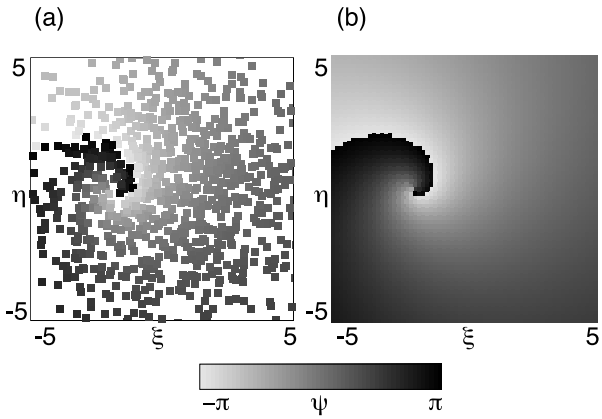

Figure 8. Validity of mapping criterion for $c = 1.5$ and $\alpha = 0.01$. The coincidence between (*a*) and (*b*) is qualitatively good even in this extraordinary example.

We have adopted this static method to the GL map neural network, and have obtained results that explain numerical simulation quite well for $c < 1.0$. However, we did not succeed in predicting the parameter dependences for $c \gtrsim 1.0$. The discrepancy becomes more enhanced as $|c|$ is increased. The lack of the Lyapunov function for $c \neq 0$ does not ensure the stability of the fixed-point solution of macroscopic variables even though SCSNA predicts the existence of the solution. The slight deviation of c from zero must cause the dynamical correlations in its dynamics, and the stable fixed-point solution at $c = 0$ bifurcates into an unstable fixed-point one and a stable periodic one. For a small c value, they are extremely close in the macroscopic variable space, but the distance between them does not remain negligible for large c. From these observations, we conclude that the SCSNA approximation is effective to explore only the unstable fixed-point solution for $c \neq 0$, and is not practical unless the intrinsic solution stays in the vicinity of the unstable one. In order to understand the whole structure of the phase diagram,

we could use dynamical theory [24, 25], taking into account the dynamical correlations of the macroscopic variables. This is now under consideration, and will be reported elsewhere.

Appendix A. Signal-to-noise analysis

We set the initial values $\boldsymbol{\theta_0} = \boldsymbol{\phi_1}$. Then the local fields at $n = 0$ are calculated as

$$h_0^{(j)} = \sum_{k=1}^{N} J_{jk} \mathrm{e}^{\mathrm{i}\phi_1^{(k)}} = \mathrm{e}^{\mathrm{i}\phi_1^{(j)}} + \frac{1}{N} \sum_{k \neq j}^{N} \sum_{\mu=1}^{p} \mathrm{e}^{\mathrm{i}(\phi_\mu^{(j)} - \phi_\mu^{(k)} + \phi_1^{(k)})}$$

where we used (2.2). The first term is called the *signal* and the second the *noise term* of $\mathrm{O}(\sqrt{\alpha})$, with the help of $\alpha = p/N$. Updating with these local fields gives

$$\begin{aligned} \mathrm{e}^{\mathrm{i}\theta_1^{(j)}} &= f(\mathrm{e}^{\mathrm{i}\phi_1^{(j)}}, \text{c.c.}) + \left[\frac{\partial f(h, h^*)}{\partial h} \mathrm{O}(\sqrt{\alpha}) + \frac{\partial f(h, h^*)}{\partial h^*} \mathrm{O}(\sqrt{\alpha}) \right] \Bigg|_{h = \mathrm{e}^{\mathrm{i}\phi^{(j)}}} \\ &= \mathrm{e}^{\mathrm{i}\phi_1^{(j)}} + \mathrm{O}(\sqrt{\alpha}) \end{aligned}$$

because of (2.1*a*), (2.1*c*) and (2.4). Thus, if the loading rate α is small enough to neglect the second and third terms in the above, pattern 1 recovers from the disturbance generated by the embedding of the other patterns.

Appendix B. Derivation of the complex SCSNA

In this appendix, we extend SCSNA [23] such that the overlap is a complex variable. Throughout this paper we are concerned with the case of $N \to \infty$. When the state of the system is in an embedded pattern $\mu = 1$ such as (4.1), the overlaps satisfy

$$|m_n^1| = \mathrm{O}(1) \qquad |m_n^\mu| = \mathrm{O}(N^{-1/2}) \qquad \text{for} \quad \mu \geqslant 2. \tag{B.1}$$

Hereafter, we restrict ourselves to dealing with the fixed-point state, and the subscript n is neglected. With the use of the overlaps, the local field is written as the sum of the signal and the noise terms as

$$h^{(j)} = \mathrm{e}^{\mathrm{i}\phi_1^{(j)}} m^1 + \sum_{\mu \geqslant 2}^{p} \mathrm{e}^{\mathrm{i}\phi_\mu^{(j)}} m^\mu.$$

The SCSNA procedure begins with the decomposition of the noise term into the systematic part $\gamma \mathrm{e}^{\mathrm{i}\theta^{(j)}}$ and the pure noise part $z^{(j)}$:

$$\sum_{\mu \geqslant 2}^{p} \mathrm{e}^{\mathrm{i}\phi_\mu^{(j)}} m^\mu = z^{(j)} + \gamma \mathrm{e}^{\mathrm{i}\theta^{(j)}}. \tag{B.2}$$

Since the updating through the above local field leads to the same solution, the next equation holds:

$$\mathrm{e}^{\mathrm{i}\theta^{(j)}} = f(\mathrm{e}^{\mathrm{i}\phi_1^{(j)}} m^1 + z^{(j)} + \gamma \mathrm{e}^{\mathrm{i}\theta^{(j)}}, \text{c.c.}). \tag{B.3}$$

This can be regarded as the equation determining $\mathrm{e}^{\mathrm{i}\theta^{(j)}}$. We assume that this can be formally solved as

$$\mathrm{e}^{\mathrm{i}\theta^{(j)}} = \tilde{f}(\mathrm{e}^{\mathrm{i}\phi_1^{(j)}} m^1 + z^{(j)}, \text{c.c.}). \tag{B.4}$$

The combination of (3.1) and (B.4) yields

$$m^1 = \frac{1}{N} \sum_{j}^{N} \mathrm{e}^{-\mathrm{i}\phi_1^{(j)}} \tilde{f}(\mathrm{e}^{\mathrm{i}\phi_1^{(j)}} m^1 + z^{(j)}, \text{c.c.}). \tag{B.5}$$

The subsequent step is to self-consistently determine γ and the statistics of $z^{(j)}$. Initially we concentrate on a specific pattern $\nu(\neq 1)$. The pure noise contains a small signal proportional to the pattern ν and the remaining term as

$$z^{(j)} = \mathrm{e}^{\mathrm{i}\phi_\nu^{(j)}} m^\nu + z^{(j),\nu} \qquad (\nu \neq 1).$$

Note that both $z^{(j)}$ and $z^{(j),\nu}$ are $\mathrm{O}(N^{-1/2})$ and that the physical difference between them could be neglected in the limit $N \to \infty$. m^ν is calculated according to the definition, and is expanded up to the first order of m^ν as

$$\begin{aligned} m^\nu &= \frac{1}{N}\sum_j^N \mathrm{e}^{-\mathrm{i}\phi_\nu^{(j)}} \tilde{f}(\mathrm{e}^{\mathrm{i}\phi_1^{(j)}} m^1 + \mathrm{e}^{\mathrm{i}\phi_\nu^{(j)}} m^\nu + z^{(j),\nu}, \text{c.c.}) \\ &= \frac{1}{N}\sum_j^N \mathrm{e}^{-\mathrm{i}\phi_\nu^{(j)}} \left[\tilde{f}(h,h^*) + \mathrm{e}^{\mathrm{i}\phi_\nu^{(j)}} m^\nu \frac{\partial \tilde{f}(h,h^*)}{\partial h} \right. \\ &\quad \left. + \mathrm{e}^{-\mathrm{i}\phi_\nu^{(j)}} m^{\nu *} \frac{\partial \tilde{f}(h,h^*)}{\partial h^*} \right]\Bigg|_{h=\mathrm{e}^{\mathrm{i}\phi_1^{(j)}} m^1 + z^{(j),\nu}}. \end{aligned}$$

Taking the complex conjugate, we get a coupled linear equation

$$\begin{pmatrix} \mathcal{A}^\nu & -\mathcal{B}^\nu \\ -\mathcal{B}^{\nu *} & \mathcal{A}^{\nu *} \end{pmatrix} \begin{pmatrix} m^\nu \\ m^{\nu *} \end{pmatrix} = \begin{pmatrix} \frac{1}{N}\sum_j^N \mathrm{e}^{-\mathrm{i}\phi_\nu^{(j)}} \tilde{f} \\ \frac{1}{N}\sum_j^N \mathrm{e}^{\mathrm{i}\phi_\nu^{(j)}} \tilde{f}^* \end{pmatrix} \tag{B.6}$$

where we define

$$\mathcal{A}^\nu = 1 - \frac{1}{N}\sum_j^N \frac{\partial \tilde{f}(h,h^*)}{\partial h}\Bigg|_{h=\mathrm{e}^{\mathrm{i}\phi_1^{(j)}} m^1 + z^{(j),\nu}} \tag{B.7}$$

$$\mathcal{B}^\nu = \frac{1}{N}\sum_j^N \mathrm{e}^{-2\mathrm{i}\phi_\nu^{(j)}} \frac{\partial \tilde{f}(h,h^*)}{\partial h^*}\Bigg|_{h=\mathrm{e}^{\mathrm{i}\phi_1^{(j)}} m^1 + z^{(j),\nu}}. \tag{B.8}$$

The solution of (B.6) is given by

$$m^\nu = \frac{\mathcal{A}^{\nu *}}{(|\mathcal{A}^\nu|^2 - |\mathcal{B}^\nu|^2)N} \sum_j^N \mathrm{e}^{-\mathrm{i}\phi_\nu^{(j)}} \tilde{f} + \frac{\mathcal{B}^\nu}{(|\mathcal{A}^\nu|^2 - |\mathcal{B}^\nu|^2)N} \sum_j^N \mathrm{e}^{\mathrm{i}\phi_\nu^{(j)}} \tilde{f}^*.$$

The randomness of $\phi_\nu^{(j)}$ yields the estimations as $\mathcal{A}^\nu = \mathrm{O}(1)$ and $\mathcal{B}^\nu = \mathrm{O}(N^{-1/2})$, and therefore

$$m^\nu = \frac{1}{\mathcal{A}^\nu N}\sum_j^N \mathrm{e}^{-\mathrm{i}\phi_\nu^{(j)}} \tilde{f}(\mathrm{e}^{\mathrm{i}\phi_1^{(j)}} m^1 + z^{(j),\nu}, \text{c.c.}) \qquad (\nu \neq 1).$$

Here taking the limit $N \to \infty$ allows us to replace $z^{(j),\nu}$ by $z^{(j)}$. Then $\mathcal{A}^\nu$ does not depend on the pattern index ν, which is written as $\mathcal{A}$. Substituting it to the left-hand side of (B.2), we get the equation

$$\begin{aligned} \sum_{\mu\geqslant 2}^p \mathrm{e}^{\mathrm{i}\phi_\mu^{(j)}} m^\mu &= \frac{1}{\mathcal{A}N}\sum_{\mu\geqslant 2} \tilde{f}(\mathrm{e}^{\mathrm{i}\phi_1^{(j)}} m^1 + z^{(j)}, \text{c.c.}) \\ &\quad + \frac{1}{\mathcal{A}N}\sum_{k\neq j}^N \sum_{\mu\geqslant 2} \mathrm{e}^{\mathrm{i}(\phi_\mu^{(j)} - \phi_\mu^{(k)})} \tilde{f}(\mathrm{e}^{\mathrm{i}\phi_1^{(k)}} m^1 + z^{(k)}, \text{c.c.}) \\ &= \frac{\alpha}{\mathcal{A}} \mathrm{e}^{\mathrm{i}\theta^{(j)}} + \frac{1}{\mathcal{A}N}\sum_{k\neq j}^N \sum_{\mu\geqslant 2} \mathrm{e}^{\mathrm{i}(\phi_\mu^{(j)} - \phi_\mu^{(k)})} \tilde{f}(\mathrm{e}^{\mathrm{i}\phi_1^{(k)}} m^1 + z^{(k)}, \text{c.c.}). \end{aligned}$$

Comparing the above with the right-hand side of (B.2), we obtain

$$\gamma = \frac{\alpha}{\mathcal{A}} \tag{B.9}$$

$$z^{(j)} = \frac{1}{\mathcal{A}N}\sum_{k\neq j}^{N}\sum_{\mu\geqslant 2} \mathrm{e}^{\mathrm{i}(\phi_\mu^{(j)}-\phi_\mu^{(k)})}\tilde{f}(\mathrm{e}^{\mathrm{i}\phi_1^{(k)}}m^1 + z^{(k)}, \text{c.c.}). \tag{B.10}$$

Equation (B.10) enables us to approximately determine the distribution of random variable $z^{(j)}$.

The site average of $z^{(j)}$, $\frac{1}{N}\sum_{j=1}^{N} z^{(j)}$, obviously vanishes, and its variance is given by

$$\sigma^2 \equiv \frac{1}{N}\sum_{j=1}^{N} z^{(j)}z^{(j)*} = \frac{1}{|\mathcal{A}|^2N^3}\sum_{j=1}^{N}\sum_{k\neq j}^{N}\sum_{\mu\geqslant 2}^{p}|\tilde{f}(\mathrm{e}^{\mathrm{i}\phi_1^{(k)}}m^1 + z^{(k)}, \text{c.c.})|^2 = \frac{\alpha}{|\mathcal{A}|^2}q \tag{B.11}$$

where we introduced a macroscopic variable

$$q = \frac{1}{N}\sum_{j=1}^{N}|\tilde{f}(\mathrm{e}^{\mathrm{i}\phi_1^{(j)}}m^1 + z^{(j)}, \text{c.c.})|^2. \tag{B.12}$$

From (B.10), it is easy to prove the isotropy of the distribution of $z^{(j)} = x^{(j)} + \mathrm{i}\, y^{(j)}$

$$\frac{1}{N}\sum_{j=1}^{N}x^{(j)}y^{(j)} = 0 \qquad \frac{1}{N}\sum_{j=1}^{N}(x^{(j)})^2 = \frac{1}{N}\sum_{j=1}^{N}(y^{(j)})^2.$$

This means, because of the central limit theorem, that $z^{(j)}$ is well approximated by the Gaussian, therefore the probability distribution takes the form $\Pr(z) \sim \exp(-|z|^2/\sigma^2)$.

Let us turn to how to calculate the function $\tilde{f}$. For this purpose we define a renormalized output Y by

$$Y(\mathrm{e}^{\mathrm{i}\phi_1^{(j)}}, z^{(j)}) \equiv \tilde{f}(\mathrm{e}^{\mathrm{i}\phi_1^{(j)}}m^1 + z^{(j)}, \text{c.c.}).$$

Substituting this into (B.3), we get the relation

$$Y(\mathrm{e}^{\mathrm{i}\phi_1^{(j)}}, z^{(j)}) = f(\mathrm{e}^{\mathrm{i}\phi_1^{(j)}}m^1 + z^{(j)} + \gamma Y(\mathrm{e}^{\mathrm{i}\phi_1^{(j)}}, z^{(j)}), \text{c.c.}). \tag{B.13}$$

Hence $\tilde{f}$ is determined such that Y satisfies (B.13).

Finally, we assume the self-averaging property, which means that the average over all sites can be replaced by the ensemble average over both pattern ϕ and noise z, i.e.,

$$\frac{1}{N}\sum_{j=1}^{N}\cdots \longrightarrow \langle\langle\cdots\rangle\rangle.$$

Note that $\langle\langle\cdots\rangle\rangle$ is the same as that given in (4.3). We neglect the correlation among the randomness of patterns and noises. After the transformation

$$r = \sigma^2\alpha \tag{B.14}$$

$$U = 1 - \mathcal{A} \tag{B.15}$$

$$\zeta = \frac{z}{\sigma} \tag{B.16}$$

equations (B.5), (B.7), (B.9) and (B.11)–(B.13) are the complex version of a set of SCSNA equations (4.2*a*)–(4.2*f*). Note that we adopt U as a macroscopic variable. Because U is originally the sum of random variables as well as m, we should pay attention to whether it has a finite value or not. For the transfer function (2.1*c*), U is readily estimated to be O(1) (see appendix C).

Appendix C. Order estimations of macroscopic variables

Let us estimate the magnitude of U for transfer function (2.1*c*). From (B.7) and (B.15), U is calculated by

$$U = \frac{1}{N}\sum_{j}^{N} \left.\frac{\partial \tilde{f}(h, h^*)}{\partial h}\right|_{h=\mathrm{e}^{\mathrm{i}\phi_1^{(j)}} m + z^{(j)}}.$$

The introduction of local field $h' = \mathrm{e}^{-\mathrm{i}\phi_1^{(j)}} h$ leads to

$$\begin{aligned} U &= \frac{1}{N}\sum_{j}^{N} \mathrm{e}^{-\mathrm{i}\phi_1^{(j)}} \left.\frac{\partial \tilde{f}(\mathrm{e}^{\mathrm{i}\phi_1^{(j)}} h', \mathrm{e}^{-\mathrm{i}\phi_1^{(j)}} h'^*)}{\partial h'}\right|_{h'=m+z^{(j)}\mathrm{e}^{-\mathrm{i}\phi_1^{(j)}}} \\ &= \frac{1}{N}\sum_{j}^{N} \left.\frac{\partial \tilde{f}(h', h'^*)}{\partial h'}\right|_{h'=m+z^{(j)}\mathrm{e}^{-\mathrm{i}\phi_1^{(j)}}}. \end{aligned} \tag{C.1}$$

Here we used (2.3). Because of the isotropy of the noise z, transforming the noise to $z'^{(j)} = z^{(j)}\mathrm{e}^{-\mathrm{i}\phi_1^{(j)}}$ makes no change in the calculation of U. Therefore all the local fields $h^{(j)}$ $(j = 1, \ldots, N)$ have common signal $m = \mathrm{O}(1)$ and site-dependent small noise $z'(j)$. The N local fields with nearly same value give nearly same contributions to U. Taking into account the normalization factor $1/N$, we consequently find U estimated in O(1). In the same way, the overlap m is calculated from (B.5) as

$$m = \frac{1}{N}\sum_{j}^{N} \tilde{f}(m + z^{(j)}\mathrm{e}^{-\mathrm{i}\phi_1^{(j)}}, \text{c.c.}). \tag{C.2}$$

According to the above discussion, m is O(1), too. This result ensures the assumption (B.1). Equations (4.6*a*) and (4.6*b*) are identical to the integral forms of (C.2) and (C.1), respectively.

References

[1] Fukai T and Shiino M 1994 *Europhys. Lett.* **26** 647
[2] Fukai T and Shiino M 1995 *Neural Comput.* **7** 529
[3] Nakamura Y, Torii K and Munakata T 1995 *Phys. Rev.* E **51** 1538
[4] Chen Z, Shuai J, Zheng J, Liu R and Wu B 1996 *Physica* A **225** 157
[5] Shuai J W, Zheng J C, Chen Z X, Liu R T and Wu B X 1997 *Physica* A **238** 23
[6] Eckhorn R *et al* 1988 *Biol. Cybern.* **60** 121
[7] Gray C M, König P, Engel A K and Singer W 1989 *Nature* **338** 344
[8] Vaadia E *et al* 1995 *Nature* **373** 515
[9] Cook J 1989 *J. Phys. A: Math. Gen.* **22** 2057
[10] Noest A J 1987 *Proc. IEEE Conf. on Neural Information Processing Systems, Neural and Synthetic* ed D Z Anderson (New York: AIP)
Noest A J 1988 *Europhys. Lett.* **6** 469
Noest A J 1988 *Phys. Rev.* A **38** R2196
[11] Okuda K 1994 unpublished
[12] Amit D J 1989 *Modeling Brain Function* (Cambridge: Cambridge University Press)
[13] Matsuno T, Imada Y, Toko K and Yamafuji K 1994 *J. Phys. Soc. Japan* **63** 4335
[14] Park K and Choi M Y 1995 *Phys. Rev.* E **52** 2907
[15] Aoyagi T and Kitano K 1997 *Phys. Rev.* E **55** 7424
[16] Jongen G, Bollé D and Coolen A C C 1998 *J. Phys. A: Math. Gen.* **31** L737
[17] Uchiyama S and Fujisaka H 1997 *Phys. Rev.* E **56** 99
[18] Yamada T and Fujisaka H 1983 *Prog. Theor. Phys.* **70** 1240
Yamada T and Fujisaka H 1984 *Prog. Theor. Phys.* **72** 885
[19] Bohr T, Pedersen A W, Jensen M H and Rand D A 1990 *Nonlinear Evolution of Spatio-Temporal Structures in Dissipative Continuous Systems* ed F H Busse and L Kramer (New York: Plenum)

[20] Hakim V and Rappel W-J 1992 *Phys. Rev.* A **46** R7347
Hakim V and Rappel W-J 1994 *Europhys. Lett.* **27** 637
[21] Nakagawa N and Kuramoto Y 1993 *Prog. Theor. Phys* **89** 313
Nakagawa N and Kuramoto Y 1994 *Physica* D **75** 74
Nakagawa N and Kuramoto Y 1995 *Physica* D **80** 307
[22] Aoyagi T 1995 *Phys. Rev. Lett.* **74** 4075
[23] Shiino M and Fukai T 1992 *J. Phys. A: Math. Gen.* **25** L375
Shiino M and Fukai T 1993 *Phys. Rev.* E **48** 867
[24] Amari S and Maginu K 1988 *Neural Netw.* **1** 63
[25] Okada M 1995 *Neural Netw.* **8** 833